Comparative Analysis of $\mu(I)$ and Voellmy-Type Grain Flow Rheologies in Geophysical Mass Flows: Insights from Theoretical and Real Case Studies

Yu Zhuang[1,2,3,4], Brian W. McArdell[5], Perry Bartelt[3,4]

[1]College of Civil Engineering, Hunan University, Changsha 410082, China

[2]Key Laboratory of Building Safety and Energy Efficiency of the Ministry of Education, Changsha 410082, China

[3]WSL Institute for Snow and Avalanche Research SLF, Davos Dorf 7260, Switzerland

[4]Climate Change, Extremes and Natural Hazards in Alpine Regions Research Centre CERC

[5]Swiss Federal Institute for Forest, Snow and Landscape Research WSL, Birmensdorf 8903, Switzerland

Corresponding author: Yu Zhuang (zhuangyu@hnu.edu.cn)

Abstract

The experimental-based $\mu(I)$ rheology is now prevalent to describe the movement of gravitational mass flows. We reinterpret the $\mu(I)$ rheology as a Voellmy-type relationship to highlight its connection to grain flow theory and demonstrate its practical applications. Using one-dimensional block modeling and two real-world case studies—the 2017 Piz Cengalo rock-ice avalanche and an experimental snow avalanche at the Swiss Vallée de la Sionne test site—we demonstrate the relationship between the dimensionless number I and the granular temperature R, establishing the equivalence between $\mu(I)$ and widely-used Voellmy-type grain flow rheologies $\mu(R)$. Results indicate that $\mu(I)$ rheology utilizes the dimensionless inertial number I to mimic contributions of granular temperature/fluctuation energy to flow behaviour. In terms of Voellmy, the $\mu(I)$ rheolgy contains a velocity-dependent turbulent friction coefficient modelling shear thinning behavior. This turbulent friction assumes the production and decay of fluctuation energy are in balance, exhibiting no difference during accelerative and depositional

phases of avalanche flow. The constant Coulomb friction coefficient prevents $\mu(I)$ rheology from accurately modeling the dispositional characteristics of actual mass flows. The modeled evolution of the snow avalanche using the $\mu(I)$ rheology is too slow, lagging 5 seconds behind the measured values. More importantly, the calculated runout extends approximately 200 meters beyond the observed limits, with significant deposit anomalies in the valley. By incorporating a non-steady production and decay of fluctuation energy in the $\mu(R)$ framework, it becomes possible to achieve a good match with both the measured velocities and the observed runout. Our results highlight the strengths and limitations of both $\mu(I)$ and Voellmy $\mu(R)$ rheologies, bolstering the theoretical foundation of mass flow modeling while revealing practical engineering challenges.

Keywords: $\mu(I)$ rheology; Voellmy-type Grain flow rheologies; Geophysical mass flows; Avalanche risk assessment

1. Introduction

Creating dependable methods to forecast the runout and deposition characteristics of geophysical mass flows stands as a fundamental challenge in natural hazard research. Long runout mass flows, like debris flows, rock/ice avalanches and snow slides, occur in complex mountain terrain and exhibit an array of complex outcomes depending on their initial material composition and dynamic interactions with the substrate. These mass movements of granular composition exhibit significant mobility, vast energy, and diverse flow patterns, posing challenges for prediction using numerical models (Crosta et al., 2007; Hürlimann et al., 2015; Iverson et al., 2015; Frigo et al., 2021; Shugar et al., 2021). A crucial element for precise modeling of their various behaviors is the development of a universal rheology capable of accurately capturing their granular motion, including long-distance travel, transitions between flow regimes, and eventual deposition.

Presently, two primary types of numerical models dominate in engineering practice: discrete element methodologies (Scaringi et al., 2018; Zhao & Crosta, 2018) and continuum approaches, often employing depth-averaged techniques (Hungr & McDougall, 2009; Christen et al., 2010). Discrete approaches simulate particle interactions, incorporating fragmentation processes, thus adeptly portraying the complex behavior of flowing granular materials (Katz et al., 2014; Zhao et al., 2017; Zhuang et al., 2023a). Nonetheless, accurately replicating the sheer volume of particles within real geophysical mass flows remains a formidable challenge, constraining their utility for solving large-scale problems due to computational constraints. Conversely, the continuum approaches treat the mass flow as a "granular fluid" consisting of particle ensembles. They utilize a series of differential equations to calculate the flow process, offering high computational efficiency (McDougall & Hungr, 2004; Christen et al., 2010; Mergili et al., 2017). Because existing continuum approaches account for the essential process of ground entrainment (Sovilla & Bartelt, 2002, Bartelt et al., 2018a), frictional heating and phase changes (Valero et al., 2015; Bartelt et al., 2018b), they are somewhat more advanced than discrete element approaches and thus have been widely used to assess mass flow hazard.

The Voellmy rheology (Voellmy, 1995) has a long tradition in the hazard mitigation community and is applied to predict the velocity and runout of avalanches and debris flows (Hungr, 1995; Schraml et al., 2015; Aaron et al., 2019; Zhuang et al., 2020). It defines the relationship $\mu(V)$=S/N as follows:

$$\mu(V) = \frac{S}{N} = \mu_s + \frac{v^2}{\xi_0 h} \tag{1}$$

where μ_s considers the Coulomb friction at "stopping", v is the flowing velocity, ξ_0 the "turbulent" friction parameter; h the flowing height. Voellmy considers μ_s to describe the "solid" behavior of the flowing mass, whereas ξ_0 represents the "fluid"-like behavior. Because the Voellmy model is grounded in clear physical principles and involves only two parameters, it is frequently used in hazard mitigation.

However, a major issue with the Voellmy model is that the travel resistance of mass flows varies significantly with the flow regime (Gruber and Bartelt, 1998). In the Voellmy model, each flow regime requires a distinct set of calibrated flow parameters; there is no universal parameter set available, rendering the Voellmy approach somewhat makeshift. To address this issue, multiple researchers have suggested incorporating the concept of granular temperature (fluctuation energy R) to accurately model the flow of granular materials across both dense and fluidized flow regimes (Haff, 1983; Jenkins & Savage, 1983; Jenkins & Mancini, 1987; Gubler, 1987; Buser & Bartelt, 2009). The term granular temperature (fluctuation energy R) originates from thermodynamics and represents the kinetic energy associated with random particle motions in the granular ensemble; it is defined based on the velocity fluctuations of individual grains (Campbell, 2006). This approach involves adding an extra differential equation to account for the generation and dissipation of kinetic energy due to random particle movements (Bartelt et al., 2006). The fluctuation energy arises from shear-work rate $\dot{W}_f$ and decays by dissipative granular interactions (Haff, 1983):

$$\frac{dR(t)}{dt} = \alpha \dot{W}_f(t) - \beta(R)R(t) \tag{2}$$

where α governs the production and β governs the decay of the fluctuation energy. It is possible to express the friction parameters (μ_s, ξ) as a function of the fluctuation energy, named $\mu(R)$ rheology. Within the Voellmy framework, the $\mu(R)$ rheology has the form (Christen et al., 2010; Zhuang et al., 2024):

$$\mu(R) = \mu_s(R) + \frac{v^2}{\xi(R)h} \tag{3}$$

where $\mu_s(R) = \mu_s e^{-\frac{R(t)}{R_0}}$, $\xi(R) = \xi_0 e^{\frac{R(t)}{R_0}}$, the parameter R_0 scales the fluctuation energy. This $\mu(R)$ rheology has the advantage of modeling shear-thinning in avalanche flows, showing a better agreement with observed front velocities and mapped deposition patterns of avalanches than the classic Voellmy

89 approach (Preuth et al., 2010; Bartelt et al., 2012).

90 Recently, the $\mu(I)$ rheology is newly proposed to describe the motion of geophysical flows. It arose
91 directly from the study of small-scale granular experiments (GDR MIDI, 2004; Jop et al., 2006):

92 $$\mu(I) = \frac{S}{N} = \mu_s + \frac{(\mu_2 - \mu_s)}{\frac{I_0}{I_n} + 1} \tag{4}$$

93 Similar to Voellmy, the model consists of two parts. The first part consists of the stopping friction μ_s.
94 The second term is controlled by the inertial number I_n, which describes the ratio of inertial forces of
95 grains to imposed forces, and is defined as (GDR MIDI, 2004):

96 $$I_n = \frac{5}{2h} \frac{vd}{\sqrt{g_z h}} \tag{5}$$

97 where d is the granule diameter and g_z the slope perpendicular component of gravity. The model
98 contains two additional constant parameters, I_0 and μ_2, which can be considered the friction at large
99 I_n. Because of its well-established experimental foundation, the $\mu(I)$ model has become popular in the
100 granular mechanics community and is applied in hazard practice (e.g., Longo et al., 2019; Liu et al.,
101 2022). Although there is broad interest and advocacy for its use, the physical implications of the $\mu(I)$
102 rheology are not completely understood, which restricts its widespread adoption.

103 In this study, we reformulate the $\mu(I)$ rheology as a Voellmy-type relationship. Through one-
104 dimensional block modeling, we investigate the equivalence and difference between the $\mu(I)$ and
105 Voellmy-type grain flow rheologies. Two historical cases—the 2017 Piz Cengalo rock-ice avalanche and
106 a snow avalanche at the Vallée de la Sionne test site in Switzerland—are further analyzed to demonstrate
107 the performance of the $\mu(I)$ rheology. The primary objective of this study is to establish the $\mu(I)$
108 rheology on a more robust theoretical framework, critically enhancing our understanding of its utility in
109 predicting the dynamics of geophysical mass flows. This endeavor is essential to establish a comparative
110 understanding of different models presently used in natural hazards practice.

2. Method and Data

2.1 Reformulation of the $\mu(I)$ rheology

The rheological model describes the relationship between the shear stress S to the normal stress N of the flowing mass. The comparison between the $\mu(V)$ and $\mu(I)$ rheologies is for practical applications intuitively made in S vs N space. Here, we vary the flow height (normal stress) and fix the velocity at a specific value to make the comparison, as presented in Fig. 1a. The quantitative and qualitative similarity between the $\mu(V)$ and $\mu(I)$ approaches in S vs N space suggests a mathematical relationship between the two models. In light of this, we have reformulated the $\mu(I)$ rheology using a Voellmy sum:

$$\mu(I) = \mu_s + \frac{v^2}{\xi(I)h} \tag{6}$$

where $\xi(I)$ characterizes the "turbulent friction" of the $\mu(I)$ model. We find:

$$\xi(I) = \frac{v\left[2\, I_0 h\sqrt{g_z h}+5vd\right]}{5(\mu_2-\mu_s)d} \tag{7}$$

Different from the constant ξ_0 value in the Voellmy, $\xi(I)$ is changing during the flowing process, and is dependent on the flowing velocity and height (Fig. 1b).

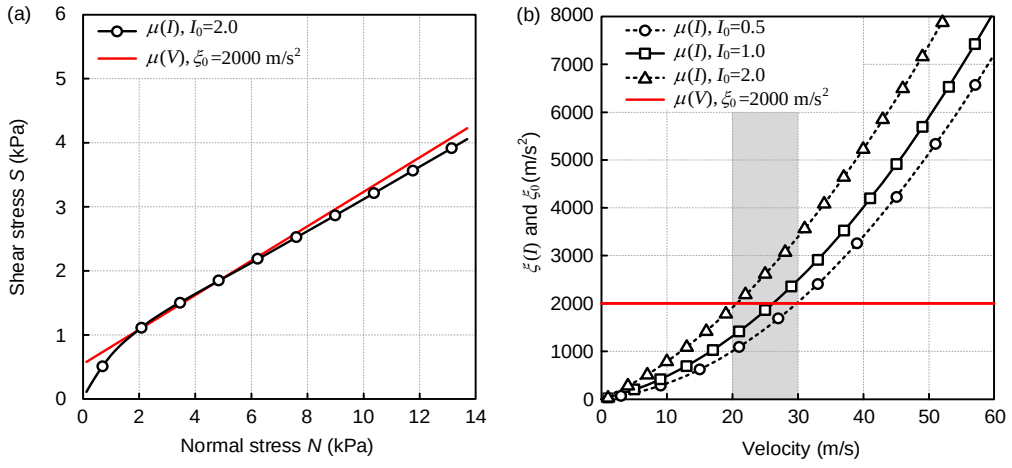

Figure 1. $\mu(I)$ vs $\mu(V)$ rheology for typical snow avalanche conditions, v=20 m/s and ρ=300 kg/m^3. For this example, we take μ_s=0.2679=tan(15^o) and μ_2=0.8391=tan(40^o). (a) The curve I_0 =2.0 plotted against $\mu(V)$ with ξ_0=2000 m/s^2. Note the strong similarity between the $\mu(I)$ and $\mu(V)$ approaches in S vs N space. (b) Comparison of the $\mu(I)$ vs $\mu(V)$ rheologies in velocity space. $\xi(I)$ increases with velocity; $\xi(V)$=ξ_0 is constant. In the shaded region 20m/s $\leq v \leq$ 30m/s, the $\xi(I)$ and $\xi(V)$ values are similar.

131 **2.2 One-dimensional block modeling analysis**

132 The turbulent friction coefficient $\xi(I)$ is velocity-dependent. According to Fig. 1, the primary reason
133 for the similarity of the two results is the selected velocity for the comparison v=20 m/s. For velocities
134 outside this range, the $\xi(I)$ and $\xi(V)$=ξ_0=constant values differ (Fig. 1b). Therefore, to investigate the
135 difference between $\mu(I)$ and $\mu(V,R)$, we must study the models over a wide range of velocities typical
136 for a specific geophysical flow from initiation to runout.

137 For this purpose, we construct a one-dimensional block model. A block of height h and mass m
138 starts from rest on a steep slope of 35° (release zone). After 30 s the block enters a transition zone of 20°,
139 where it begins to decelerate. After 90 s the block enters a flat runout zone and stops. We calculate the
140 speed and location of the block's center-of-mass; friction is given by $\mu(I)$, $\mu(V)$ and $\mu(R)$. The
141 governing ordinary differential equations for this model are:

142 $$\frac{\mathrm{d}x(t)}{\mathrm{d}t} = v(t) \tag{8}$$

143 $$\frac{\mathrm{d}v(t)}{\mathrm{d}t} = g_x(t) - \mu(I,V,R)g_z(t) \tag{9}$$

144 where $x(t)$ is the flowing distance, $v(t)$ is the flowing velocity, and (g_x, g_z) are the components of
145 gravity acceleration.

146 We consider the motion of the center-of-mass to represent the motion of a granular, geophysical
147 flow. Such simple, one-dimensional sliding block models of avalanche flow have been used extensively
148 to calculate hazard maps (Perla et al., 1980). This approach allows us to compare the $\mu(I)$ and $\mu(V,R)$
149 rheologies in velocity space.

150 **2.3 Case study of historical avalanches**

151 According to the reformulation of the $\mu(I)$ rheology, $\xi(I)$ parameter is a function of both flowing height
152 and velocity (Eq. 7), which is heavily dependent on the flowing regime and entrainment process. The

one-dimensional block model ignores the above essential features and processes. Therefore, we conduct an analysis of two historical avalanche cases: 2017 Piz Cengalo rock-ice avalanche (Mergili et al., 2020) and a snow avalanche (No. #20163017) that occurred in Vallée de la Sionne test site, Switzerland (Sovilla et al., 2018). The Piz Cengalo avalanche occurred on 23th August, 2017 with a released rock volume of ~3×10^6 m^3. The sliding mass entrained the glacial of 6×10^5 m^3 and formed a rock-ice avalanche. This avalanche is well documented with laser scans of release and deposits, providing natural materials to confirm the numerical model (Mergili et al., 2020; Walter et al., 2020). The snow avalanche (#20163017) was artificially triggered on 18th January, 2016. The avalanche involved an initial volume of 86560 m^3 and a runout of ~2500 m. The difference between DEMs before and after the event indicated the deposit structure, and cameras recorded the evolution of the snow avalanche. Detailed information about this particular snow avalanche is presented in Sovilla et al., (2018).

We implement the Voellmy $\mu(V)$, $\mu(I)$ and $\mu(R)$ rheologies into a continuum approach-based model RAMMS (Christen et al., 2010; Bartelt et al., 2018b; Zhuang et al., 2024) to elucidate the performance and limitations of the $\mu(I)$ rheology in calculating the evolution of geophysical mass flows. Detailed information about the well-established **RAMMS** model can be found in Christen et al. (2010), Bartelt et al. (2016, 2018b), and Zhuang et al. (2024).

3. Results

3.1 Rheology comparison using the one-dimensional block model

(1) The $\mu(I)$ and $\mu(V)$ rheologies in velocity space

The direct comparison of $\mu(I)$ and $\mu(V)$ reveals that both models can produce similar runout (Fig. 2a), and velocity (Fig. 2b). However, the $\mu(V)$ approach reaches a smaller peak velocity at the end of the release zone but decelerates less strongly in the transition zone (Fig. 2b). In the end, the velocity at the

beginning of the runout zone is higher. This result can also be visualized in the depiction of location through time (Fig. 2a). The Voellmy flow reaches the same runout distance but lags the $\mu(I)$ model along the intermediate transition segment. Of interest is a direct comparison of $\mu(I)$ and $\mu(V)$ through time (Fig. 2c). The $\mu(V)$ with constant ξ_0 reaches larger values (lower velocities) but decreases rapidly during the transition to the flatter 20° slope, falling to values smaller than $\mu(I)$. Both models predict the same μ values as the block enters the flat runout zone. According to Eq. 7, $\xi(I)$ increases with the flowing velocity, indicating a shear-thinning type of behavior and therefore a smaller resistance in the acceleration stage. The general model behavior over the three slope segments can be explained by the fact that the constant ξ_0 value characterizes a mean value within the domain of possible $\xi(I)$ values. Model parameters can be selected such that similar results are obtained; experiments are required to determine which accelerative/decelerative behavior represents the best fit to observations. However, there is a method to bring the two model approaches into equivalence.

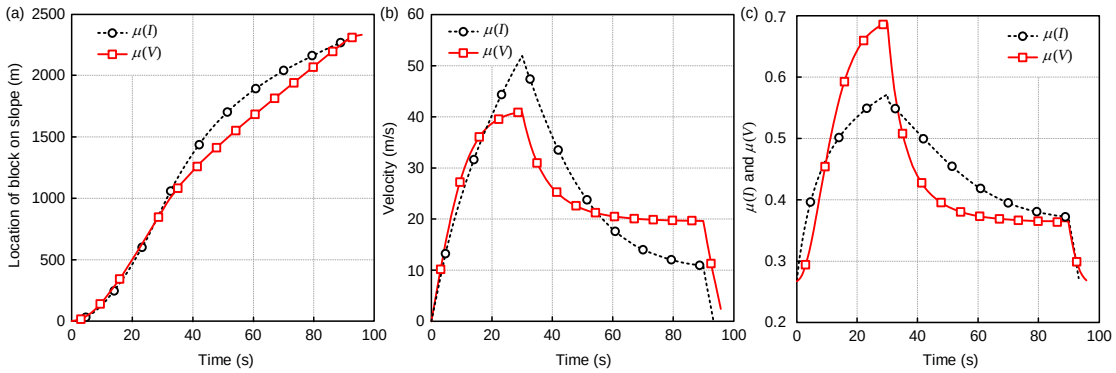

Figure 2. The $\mu(I)$ vs $\mu(V)$ rheologies in velocity space. (a) Location of center-of-mass over time. In the transition zone the Voellmy model with constant ξ_0 lags the $\mu(I)$ model. (b) Velocity over time. With a constant ξ_0 the Voellmy model tends to a steady velocity, albeit a lower velocity than $\mu(I)$. At the end of the transition zone, the Voellmy model predicts a higher (steady state) velocity. (c) *S*/*N* for $\mu(I)$ and $\mu(V)$. The Voellmy model predicts higher friction before entering the transition zone.

(2) The Voellmy grain-flow equivalent to $\mu(I)$: The $\mu(R)$ grain flow rheology

The Voellmy-type $\mu(R)$ rheology is a function of granular temperature/fluctuation energy, which arises from shearing work and decays by dissipative granular interactions. To better compare the $\mu(I)$ and

196 $\mu(R)$ rheologies, we made the Coulomb friction parameter $\mu_s(R)$ a constant but turbulent friction
197 parameter $\xi(R)$ a function of fluctuation energy, so that the two rheologies are in the same Voellmy-
198 type. When we re-solve the ordinary differential equations (Eqs. 8 and 9) with the additional production-
199 decay equation (Eq. 2) and the parameters α =0.05, β =0.95, ξ_0 =500 m/s^2 and R_0 =6 kJ, we find a
200 remarkable duplication of the $\mu(I)$ results, with regard to the calculated location (Fig. 3a), velocity (Fig.
201 3b) and calculated $\mu(I)$ and $\mu(R)$ (Fig. 3c). In this comparison the $\mu(I)$ model employed the
202 following parameters, I_0 =1.0, d =0.07 m, μ_2 =tan(40^o) and μ_s =tan(15^o).

203 These results suggest that the empirical I_n function mimics the production and decay of the
204 granular temperature R. Indeed, there is a strong qualitative similarity between the calculated I_n and
205 R functions. When the two dimensionless parameters I_n/I_0 and R/R_0 are plotted over time (Fig. 3d) or as
206 a function of the calculated velocity (Fig. 3e) there is both a strong qualitative and quantitative agreement.
207 Because I_n is a pure function of velocity (for a constant height), the calculated friction $\mu(I)$ exhibits
208 no change during the accelerative and decelerative phases of the flow: it ascends and descends on the
209 same path (Fig. 3f). In contrast, because R is a result of a production/decay equation it exhibits a
210 hysteresis (the friction does not follow the same path in the accelerative/decelerative phases of the flow).

211 Hysteresis effects have been observed in experiments with granular materials (Platzer et al., 2004;
212 Bartelt et al., 2007) and grain flows of snow (Platzer et al., 2007, Bartelt et al., 2015). They indicate a
213 process-dependent flow rheology that cannot be described by rheologies with constant flow parameters
214 (e.g., $\mu(V)$). They suggest that the friction must change as the state of the flow changes, for example as
215 the grain flow continuum changes velocity. The correspondence between $\mu(I)$ and $\mu(R)$ models
216 underscores the importance of embracing randomness and temporal evolution in the modeling of granular
217 flows.

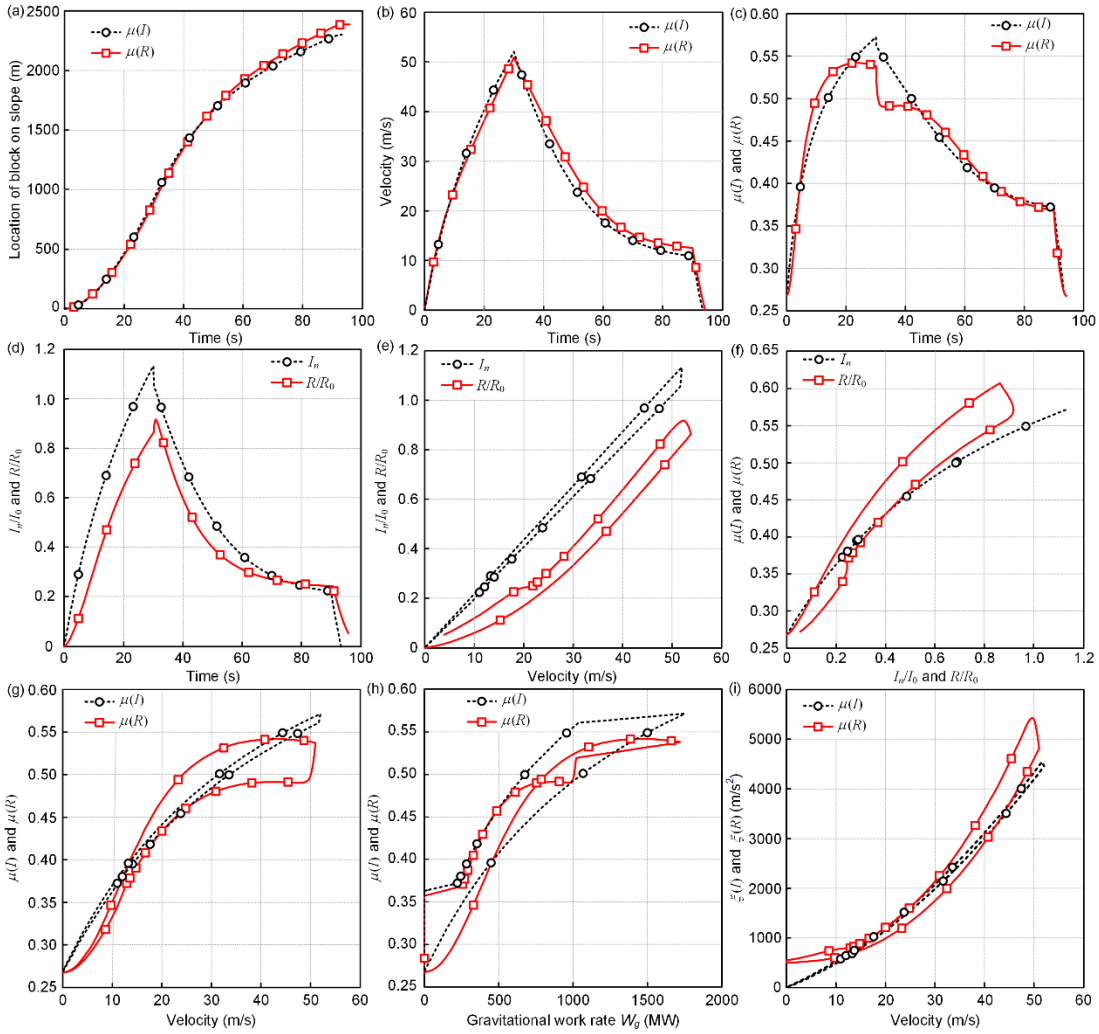

Figure 3. Comparison between the $\mu(I)$ vs $\mu(R)$ rheologies. (a)-(c) show the calculated location of center-of-mass, velocity and friction of the two rheologies. (d)-(e) Comparison between I_n/I_0 and R/R_0 over time and flow velocity. (f) Calculated friction $\mu(I)$ vs $\mu(R)$ as a function of I_n/I_0 and R/R_0. (g)-(h) Calculated $\mu(I)$ vs $\mu(R)$ as a function of the velocity and gravitational work rate. (i) Comparison between $\xi(I)$ (Eq. 7) and $\xi(R)$.

Both $\mu(I)$ and $\mu(R)$ rheologies exhibit hysteresis in terms of velocity (Fig. 3g) or gravitational work rate (Fig. 3h). Although the $\mu(I)$ friction expressed in terms of I_n/I_0 exhibits no hysteresis (Fig. 3f), the $\mu(I)$ rheology in terms of velocity and gravitational work rate does. However, this dependency is much more prominent in the $\mu(R)$-type rheologies because it is governed by two processes-both the production of fluctuation energy and its eventual decay. The $\mu(I)$ approach models the net production, always assuming that the two are in balance. During slope transitions, or other flow states in which production and decay are out-of-balance, this might not be the appropriate description. This is why the

most apparent differences between $\mu(I)$ and $\mu(R)$ arise during slope transitions. Despite these differences, however, there is a strong correlation between $\mu(I)$ and $\mu(R)$. For example, when we depict the calculate $\xi(I)$ and $\xi(R)$ function in terms of velocity there is almost a one-to-one agreement in the numerical values (Fig. 3i). The only significant difference is that the $\mu(I)$ rheology predicts an infinite friction ($\xi(I)$=0) at the velocity of zero, whereas the $\mu(R)$ approach predicts some finite value (in this case when R=0, $\xi(R)$=ξ_0).

3.2 Rheology comparison using real case studies

(1) Piz Cengalo rock-ice avalanche

We apply the $\mu(I)$, $\mu(V)$, and $\mu(R)$ rheologies to calculate the dynamics of the Piz Cengalo rock-ice avalanche and the Vallée de la Sionne snow avalanche (Sovilla et al., 2018). Modeling parameters and results for the Piz Cengalo avalanche are presented in Fig. 4. The $\mu(R)$ parameters are empirical values, which arise from numerous practical experiences and have been widely used in rock-ice avalanche research (Munch et al., 2024; Zhuang et al., 2024). The input parameters ($\mu_{s,rock}$, $\mu_{s,ice}$, $\xi_{s,rock}$, $\xi_{s,ice}$) represent the frictional parameters for a dense, granular packing of rock-ice mixture. Here, the Columb and turbulent friction coefficients <$\mu_s(R)$, $\xi(R)$> are both functions of the fluctuation energy. In the $\mu(I)$ rheology, I_0=0.3 is a typical value from Pouliquen & Forterre (2002), Forterre & Pouliquen (2003), and Jop et al. (2006), d=1.0 m and μ_2=tan(40°)=0.839 arise from field investigations of particle size and deposit distribution. The μ_s value and parameters in the $\mu(V)$ rheology are determined from inversion analysis that the calculated avalanche runout matches the actual condition. For ease of comparison, the same Coulomb friction coefficients are applied in the $\mu(I)$ and $\mu(V)$ rheologies. The sensitivity analysis of parameters in the $\mu(I)$ and $\mu(V)$ rheologies are well presented (Iannacone et al., 2013; Argentin et al., 2022; Zhao et al., 2024; Zhuang et al., 2023b) and are not performed here.

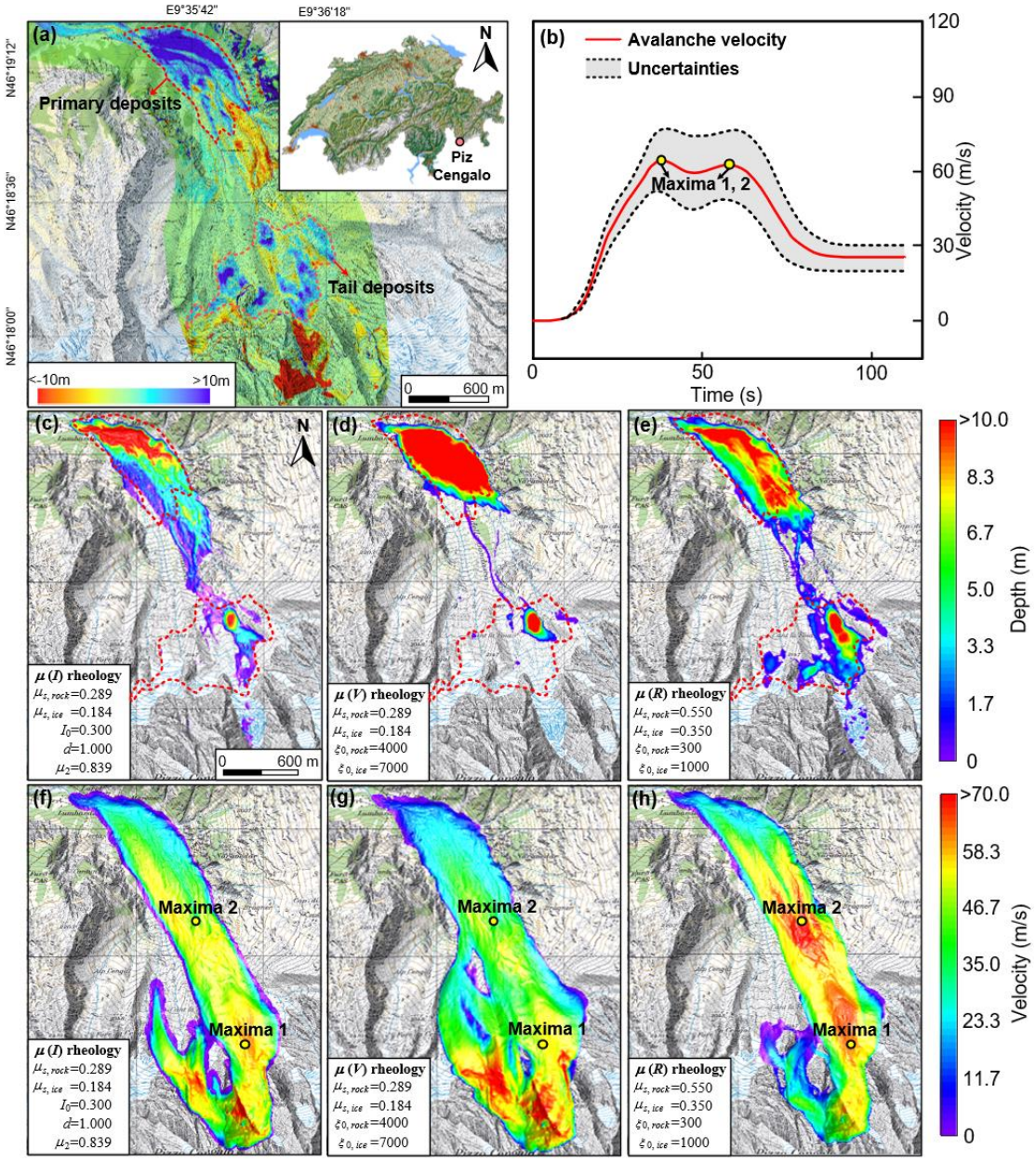

Figure 4. Rheology comparation with the Piz Cengalo rock-ice avalanche. (a) Deposit structure arises from the laser scans. The grid represents the longitude and latitude of the study area. (b) Seismic signal analysis of the avalanche velocity, derived by Walter et al. 2020. (c)-(e) Modeled avalanche deposits with different rheologies. (4) Modeled avalanche velocity with different rheologies. Two maxima represent the locations derived by seismic signal analysis.

Modeling results of all three rheologies exhibit satisfactory runout distance, but there are deviations in the calculated deposit structure and avalanche velocity. Laser scans indicate two deposit areas of the Piz Cengalo avalanche (Fig. 4a): a primary deposit area of ~2×10^5 m^2 at the mountain toe (1350-1450 m a.s.l.) and tail deposits spread on the steep slope (2000 m-2250 m a.s.l.). Both $\mu(I)$ and $\mu(V)$ models

make a deposit anomaly at the mountain toe (Fig. 4 c and d), exceeding the measurements considerably. Very few deposits remained on the steep slope, resulting in significantly smaller accumulation area and thickness compared to the actual condition. Conversely, modeling deposits of the $\mu(R)$ model exhibits a reasonable deposit structure, whether in the primary deposit area or on the steep slope (Fig. 4e). To align the calculated avalanche runout with the actual condition, small Columb friction μ_s, which is dominant when the avalanche comes close to stopping, is applied in the $\mu(I)$ and $\mu(V)$ models. This modification dictates the final runout accumulation, leading to deposits primarily concentrated on areas with gentle slopes, while leaving smaller deposits on steeper inclines. According to the seismic signal analysis (Fig. 4b, Walter et al., 2020), the Piz Cengalo avalanche has a duration of ~100 s and a maximum velocity of 64 m/s. There are two avalanche velocity maxima: the first reaches when the avalanche leaves the steep glacier portion, and the second occurs behind the steep terrain step in the central runout area. The mean velocity between the two maxima is 40-60 m/s. The analysis comparing modeled avalanche velocities and seismic signals indicates that the $\mu(R)$ rheology outperforms others in terms of peak values and velocity evolution, as shown in Fig. 4h. Seismic signal analysis, representing the average velocity of the mass center, explains why a slightly higher peak velocity is observed in the modeling results. In contrast, the $\mu(I)$ and $\mu(V)$ rheologies display higher velocities downstream from the source area but show reduced velocities in the transition and deposition areas, deviating from actual conditions as depicted in Figs. 4f and 4g. The small Columb friction μ_s and high ξ_0 value impart the avalanche with high mobility in the initial stage. This result is also visualized in the modeled deposit distribution that very few materials are deposited on the steep slope.

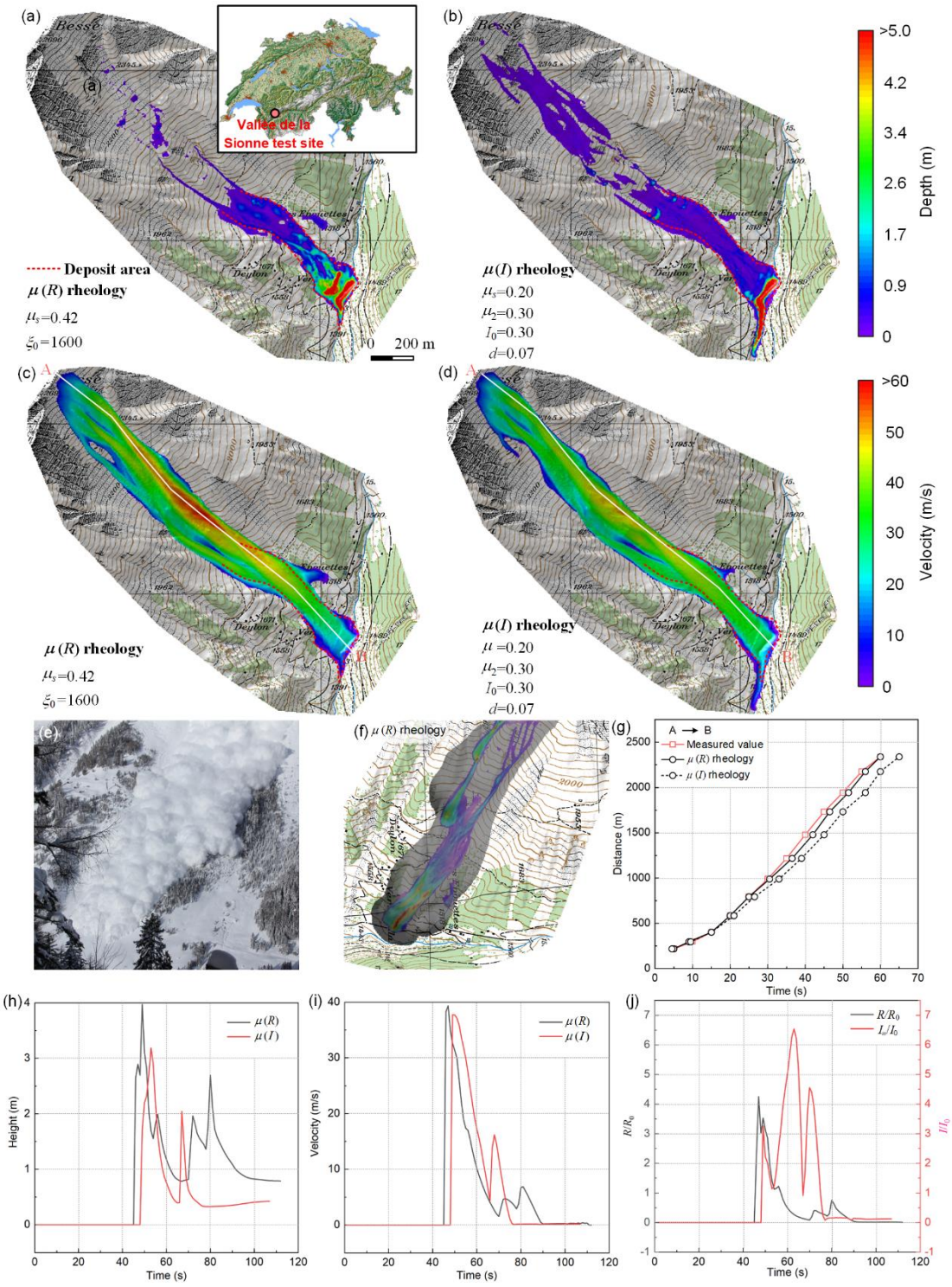

Figure 5. Modeling results of the Vallée de la Sionne snow avalanche (#20163017). (a)-(d) show the simulated avalanche deposits and velocity with the two rheologies. The grid represents the longitude and latitude of the study area. (e)-(f) show the comparison between recorded videos and modeling results of the $\mu(R)$ rheology. (g) Comparison between measured avalanche evolution with modeling results. The profile AB is presented in Fig. 5c-d (h)-(i) The simulated height and velocity of the mass centre with the two rheologies. (j) Comparison between R/R_0 and I_n/I_0.

(2) Vallée de la Sionne snow avalanche (#20163017)

For the analyzed snow avalanche, the modeling parameters were calibrated to align the simulated avalanche evolution and velocity with the measured values. The progression of the avalanche front was recorded at fixed time intervals of 5 seconds, providing a basis for comparison. The modeling parameters and results for the $\mu(I)$ and $\mu(R)$ rheologies are illustrated in Fig. 5.

Both rheological models capture the avalanche's evolution and velocity satisfactorily, though the rheology underestimates the timing by approximately 5 seconds compared to the actual conditions (Fig. 5c, d, and g). Yet, profound differences $\mu(I)$ emerge when examining the simulated runout distance and deposit structure. In the $\mu(R)$ rheology, the avalanche achieves a runout distance of approximately 2500 meters. The deposits are concentrated at the mountain's toe, where the slope transitions to a gentler incline, closely mirroring field observations (Fig. 5a, e, and f).

In contrast, the $\mu(I)$ rheology exhibits significantly different behavior. The avalanche does not stop at the mountain's toe but continues moving into the valley, showing excessive mobility (Fig. 5b). The sliding mass bulks unnaturally in the valley, and the deposit depth greatly exceeds observed conditions. This divergence arises from the Coulomb friction coefficient μ_s used in the $\mu(I)$ rheology. To match the measured velocity, a smaller μ_s value was applied, resulting in an extended runout and deposition in the flatter terrain of the valley.

Further insight emerges when contrasting R/R_0 with and I_n/I_0, as shown in Fig. 5j. The scaling factors R_0 and I_0 encapsulate the influence of sliding materials. While R_0 =2 kJ/m^3 represents a typical value for snow avalanches (Buser & Bartelt, 2015), I_0 is derived from laboratory experiments using glass beads (Forterre & Pouliquen, 2003; Jop et al., 2006). This disparity in scaling reflects the intrinsic differences in material behavior and introduces a subtle, yet significant, divergence in

rheological interpretation.

Through this analysis, we observe that the $\mu(R)$ rheology, with its non-steady production and dissipation of fluctuation energy, achieves a more faithful reproduction of both the avalanche's dynamics and deposition patterns, underscoring the nuanced interplay of microscopic and macroscopic principles in granular flow systems.

4. Discussion and Implications

With this contribution, we strengthen the theoretical foundation of the $\mu(I)$ rheology. It has an equivalence with the Voellmy-type grain flow rheologies, which are composed of a Coulomb stopping friction and a turbulent friction that controls the flow velocity. Compared with the classic $\mu(V)$ rheology of constant friction parameters, an advantage of the $\mu(I)$ rheology is to define the turbulent friction parameter $\xi(I)$ as a function of flowing velocity and height (using inertial number I_n). This modification incorporates the shear-thinning behavior (Hu et al., 2022) and the impact of volume (where increased normal stress results in a reduced friction coefficient, see Heim, 1932; Wang et al., 2018), capturing key characteristics of these phenomena. With the help of grain flow theory (Haff, 1983, Jenkins & Savage, 1983; Buser & Bartelt, 2009), we find the contribution of I_n attributes to its empirical representation of the granular temperature/fluctuation energy R. However, the inertial number I_n is just a function of flowing velocity, assuming the production and decay of the fluctuation energy are in balance. The $\mu(I)$ rheology, therefore, exhibits no change during the acceleration and deceleration process, leading to the deviation of calculated velocity for real case studies.

Though the $\mu(I)$ rheology demonstrates an improvement over the classic $\mu(V)$ rheology, it has a critical flaw in ignoring the contribution of fluctuation energy to the Coulomb friction coefficient μ_s. In the $\mu(I)$ rheology, the constant μ_s value makes the sliding mass stop on a single slope angle

(arctan(μ_s)). Consequently, the modeled deposits of the Piz Cengalo avalanche and Vallée de la Sionne snow avalanche concentrate at the mountain toe, with very few materials deposit on the slope. Considering that avalanche deposits in real-world scenarios often cover a broad area with varying thicknesses, using a constant μ_s value is unlikely to yield an accurate representation of the deposit structure.

A significant challenge in landslide risk assessment is to establish reliable numerical parameters, highlighting a limitation in both the $\mu(I)$ and classic $\mu(V)$ rheologies: the reliance on input parameters derived from inversion analysis (Zhao et al., 2024). Although the $\mu(I)$ rheology is based on experimental data, relevant experiments are limited, and the test materials used are predominantly glass beads (Foterre & Pouliquen, 2003; Jop et al., 2006). To date, no large-scale experiments have been conducted on geophysical mass flows, to our knowledge. Considering the substantial differences in properties among materials in the flowing mass, such as rock, ice, snow, and water, it proves highly challenging to accurately characterize avalanche motion using a uniform surrogate material with different properties, such as glass. Additionally, the dynamics of avalanches are greatly influenced by the flow regime and topography, indicating that avalanches composed of the same material can display varied runout lengths and deposit patterns under different conditions.

This phenomenon further complicates the task of selecting appropriate model parameters. In this study, to achieve a satisfactory runout of the Piz Cengalo avalanche and a reasonable velocity of the Vallée de la Sionne snow avalanche, small μ_s values arise from inversion analysis are applied for the calculation of $\mu(I)$ and $\mu(V)$ models. We admit that model parameters can be calibrated such that realistic runout or velocity are obtained, but these site-specifically calibrated parameters limit the engineering application of the model, particularly when conducting risk assessments of potential

avalanches. The existing $\mu(R)$ model offers a possible solution (Christen et al., 2010; Bartelt et al., 2011; Zhuang et al., 2023c). By defining the Coulomb stopping friction and turbulent friction parameters as functions of fluctuation energy, we can characterize the effects of flow regime and topography changes on the friction of landslides (Preuth et al., 2010). Using a group of empirical parameters, which represent the material properties of rock, ice and snow, realistic deposit structure and velocity evolution can be obtained. Because R represents the energy associated with random particle motions, it introduces an element of stochasticity into avalanche modelling. Clearly, it is impossible to precisely determine the position of every individual particle in an avalanche, contrary to what Discrete Element Modeling (DEM) might imply. Nonetheless, the behavior of the granular ensemble seems to be directed by a production/decay equation, which, even when estimated approximately, can impart a discernible trajectory to the avalanche process and deposition dynamic, thereby enhancing the predictive accuracy of numerical models.

Further case studies on various types of geophysical mass flows, such as rock avalanches, ice avalanches, and snow avalanches, will help quantify the modeling parameters of $\mu(R)$ rheology (production and decay of fluctuation energy) with less uncertainty. The remaining challenge is to formulate a comprehensive rheology that incorporates the critical physical processes involved in mass flows, including water lubrication, fluidization, sliding materials, and ground roughness.

5. Conclusion

In this paper, we describe the equivalence and difference between three widely-used rheologies to model geophysical mass flows: (1) the classic Voellmy rheology, (2) $\mu(I)$ rheology and (3) $\mu(R)$ rheology. The $\mu(I)$ rheology can be reformulated as Voellmy-type, which is composed of a Coulomb and a turbulent friction term. Different from the classic Voellmy rheology (constant ξ value), $\mu(I)$ rheology

involves a velocity-dependent ξ parameter, modeling a shear-thinning behavior. It utilizes a dimensionless inertial number I_n to minic contributions of fluctuation energy to the runout behavior of mass flows, building an equivalence with the $\mu(R)$ rheology. Though both $\mu(I)$ and $\mu(R)$ models indicate that friction is a process, changing in time and space, the $\mu(I)$ rheology assumes the production and decay of fluctuation energy are in balance, exhibiting the same friction behavior during the accelerative and depositional phases. More importantly, a critical flaw of the $\mu(I)$ rheology is suggesting a constant Colomb friction, ignoring the impacts of fluctuation energy on the Colomb stopping friction. Modeled avalanche deposits of the Piz Cengalo rock-ice avalanche and the Vallée de la Sionne snow avalanche are both concentrated in areas with gentle slopes. The existing $\mu(R)$ rheology makes up for the shortcomings, exhibiting good performance in predicting the deposit patterns of geophysical mass flows. These insights have practical implications for improving geophysical flow models, offering a more comprehensive understanding of flow behavior and its dependence on factors such as velocity, terrain features, and material properties. As we continue to refine our models, we move closer to more accurate assessments and mitigation of geophysical hazards.

Data availability

No data sets were used in this article.

Author contribution

Yu Zhuang did the numerical work and wrote the manuscript with contributions from all co-authors. Perry Bartelt designed the work, did the calculation and wrote the manuscript. Brian W. McArdell edited the manuscript.

Competing interests

401 The authors declare that they have no known competing financial interests or personal relationships that
402 could have appeared to influence the work reported in this paper.

403 **Acknowledgments**

404 This study is supported by the RAMMS project and the Fundamental Research Funds for the Central
405 Universities.

406 **References**

407 Aaron, J., McDougall, S., and Nolde, N.: Two methodologies to calibrate landslide runout models,
408 Landslides, 16(5), 907-920, 2019.
409 Argentin, A. L., Hauthaler, T., Liebl, M., Robl, J., Hergarten, S., Prasicek, G., Salcher, B., Hölbling, D.,
410 Pfalzner-Gibbon, C., Mandl, L., Maroschek, M., Abad, L., and Dabiri, Z.: Influence of rheology on
411 landslide-dammed lake impoundment and sediment trapping: Back-analysis of the Hintersee
412 landslide dam, Geomorphology, 414, 108363.,
413 Bartelt, P., Buser, O., and Platzer, K.: Fluctuation-dissipation relations for granular snow avalanches,
414 Journal of Glaciology, 52(179), 631-643, 2006.
415 Bartelt, P., Buser, O., and Platzer, K.: Starving avalanches: frictional mechanisms at the tails of finite-
416 sized mass movements, Geophysical Research Letters, 34(20), 1-6, 2007.
417 Bartelt, P., Meier, L., and Buser, O.: Snow avalanche flow-regime transitions induced by mass and
418 random kinetic energy fluxes, Annals of Glaciology, 52(58), 159-164, 2011
419 Bartelt, P., Bühler, Y., Buser, O., Christen, M., and Meier, L.: Modeling mass-dependent flow regime
420 transitions to predict the stopping and depositional behavior of snow avalanches, Journal of
421 Geophysical Research, 117, F01015, 2012.
422 Bartelt, P., Vera Valero, C., Feistl, T., Christen, M., Bühler, Y., and Buser, O.: Modelling cohesion in snow

avalanche flow, Journal of Glaciology, 61(229), 837-850, 2015.

Bartelt, P., Christen, M., Bühler, Y., Caviezel, A., and Buser, O.: Snow entrainment: Avalanche interaction with an erodible substrate, Proceedings, International Snow Science Workshop, 716-720, 2018a.

Bartelt, P., Christen, M., Bühler, Y., and Buser, O.: Thermomechanical modelling of rock avalanches with debris, ice and snow entrainment, Numerical Methods in Geotechnical Engineering, IX, 1047-1054, 2018b.

Buser, O., and Bartelt, P.: Production and decay of random kinetic energy in granular snow avalanches, Journal of Glaciology, 55, 3-12, 2009.

Buser, O., and Bartelt, P.: An energy-based method to calculate streamwise density variations in snow avalanches. Journal of Glaciology, 61(227), 563-575, 2015.

Campbell, C. S.: Granular material flows-An overview, Powder Technology, 162, 208-229, 2006.

Christen, M., Kowalski, J., and Bartelt, P.: RAMMS: Numerical simulation of dense snow avalanches in three-dimensional terrain, Cold Regions Science and Technology, 63(1-2), 1-14, 2010.

Crosta, G. B., Frattini, P., & Fusi, N.: Fragmentation in the Val Pola rock avalanche, Italian Alps, Journal of Geophysical Research: Earth Surface, 112(F1), F01006, 2007.

Forterre, Y., and Pouliquen, O.: Long-surface-wave instability in dense granular flows, Journal of Fluid Mechanics, 486, 21-50, 2003.

Frigo, B., Bartelt, P., Chiaia, B., Chiambretti, I., and Maggioni, M.: A reverse dynamical investigation of the catastrophic wood-snow avalanche of 18 January 2017 at Rigopiano, Gran Sasso National Park, Italy, International Journal of Disaster Risk Science, 12, 40-55, 2021.

GDR, MiD.: On dense granular flows, The European Physical Journal E, 14, 341-365, 2004.

Gruber, U., and Bartelt, P.: Avalanche hazard mapping using numerical Voellmy-fluid models, 1998.

Gubler, H.: Measurements and modelling of snow avalanche speeds, IAHS Publ. 162 (Symposium at Davos 1986-Avalanche Formation, Movement and Effects), 405-420, 1987.

Haff, P. K.: Grain flow as a fluid-mechanical phenomenon, Journal of Fluid Mechanics, 134, 401-430, 1983.

Heim, A.: Bergsturz und Menschenleben. Beiblatt zur Vierteljahrsschrift der Naturforschenden Gesellschaft Zürich, 20, 217: 1932

Hu, W., Li, Y., Xu, Q., Huang, R. Q., McSaveney, M., Wang, G. H., Fan, Y., Wasowski, J., and Zheng, Y. S.: Flowslide High Fluidity Induced by Shear Thinning, Journal of Geophysical Research: Solid Earth, 127, e2022JB024615, 2022.

Hungr, O.: A model for the runout analysis of rapid flow slides, debris flows, and avalanches, Canadian Geotechnical Journal, 32(4), 610-623, 1995.

Hungr, O., and McDougall, S.: Two numerical models for landslide dynamic analysis. Computers & Geosciences, 35(5), 978-992, 2009.

Hürlimann, M., McArdell, B. W., & Rickli C.: Field and laboratory analysis of the runout characteristics of hillslope debris flows in Switzerland, Geomorphology, 232, 20-32, 2015.

Iannacone, J. P., Luna, B. Q., and Corsini, A.: Forward simulation and sensitivity analysis of run-out scenarios using MassMov2D at the Trafoi rockslide (South Tyrol, Italy), Georisk: Assessment and Management of Risk for Engineered Systems and Geohazards, 7(4), 240-249, 2013.

Iverson, R. M., George, D. L., Allstadt, K., Reid, M. E., Collins, B. D., Vallance, J. W., Schilling, S. P., Godt, J. W., Cannon, C. M., Magirl, C. S., Baum, R. L., Coe, J. A., Schulz, W. H., and Bower, J. B.: Landslide mobility and hazards: implications of the 2014 Oso disaster, Earth and Planetary Science Letters, 412, 197-208, 2015.

467 Jenkins, J. T., and Savage, S. B.: A theory for the rapid flow of identical, smooth, nearly elastic particles.
468 Journal of Fluid Mechanics, 136, 186-202, 1983.
469 Jenkins, J. T., and Mancini, F.: Plane flows of a dense, binary mixture of smooth, nearly elastic circular
470 disks, Journal of Applied Mechanics, 54(1), 27-34, 1987
471 Jop, P., Forterre, Y., and Pouliquen, O.: A constitutive law for dense granular flows, Nature, 441(7094),
472 727-730, 2006.
473 Katz, O., Morgan J. K., Aharonov, E., and Dugan, B.: Controls on the size and geometry of landslides:
474 Insights from discrete element numerical simulations, Geomorphology, 220, 104-113, 2014.
475 Liu, Z., Fei, J., and Jie, Y.: Including μ (I) rheology in three-dimensional Navier-Stokes-governed
476 dynamic model for natural avalanches, Powder Technology, 396, 406-432, 2022.
477 Longo, A., Pastor, M., Sanavia, L., Manzanal, D., Martin Stickle, M., Lin, C., Yague, A., and Tayyebi,
478 S.M.: A depth average SPH model including μ (I) rheology and crushing for rock avalanches,
479 International Journal for Numerical and Analytical Methods in Geomechanics, 43(5), 833-857, 2019.
480 McDougall, S., and Hungr, O.: A model for the analysis of rapid landslide motion across three-
481 dimensional terrain, Canadian Geotechnical Journal, 41(6), 1084-1097, 2004.
482 Mergili, M., Fischer, J. T., Krenn, J., and Pudasaini, S. P.: r.avaflow v1, an advanced open-source
483 computational framework for the propagation and interaction of two-phase mass flow, Geoscientific
484 Model Development, 10, 553-569, 2017.
485 Mergili, M., Jaboyedoff, M., Pullarello, J., and Pudasaini, S. P.: Back calculation of the 2017 Piz
486 Cengalo-Bondo landslide cascade with r.avaflow: what we can do and what we can learn, Natural
487 Hazards and Earth System Sciences, 20, 505-520, 2020.
488 Munch, J., Zhuang, Y., Dash, R. K., and Bartelt, P.: Dynamic Thermomechanical Modeling of Rock-Ice

Avalanches: Understanding Flow Transitions, Water Dynamics, and Uncertainties, Journal of Geophysical Research: Earth Surface, 129, e2024JF007805, 2024.

Perla, R., Cheng, T. T., and McClung, M. D.M.: A Two-Parameter Model of Snow-Avalanche Motion, Journal of Glaciology, 26, 197-207, 1980

Platzer, K. M., Margreth, S., and Bartelt, P.: Granular flow experiments to investigate dynamic avalanche forces for snow shed design. In P. Bartelt, E. Adams, M. Christen, R. Sack, & A. Sato (Eds.), Snow engineering V, Proceedings of the fifth international conference on snow engineering, 5-8 July 2004, Davos, Switzerland (pp. 363-370), 2004.

Platzer, K., Bartelt, P., and Kern, M.: Measurements of dense snow avalanche basal shear to normal stress ratios (S/N), Geophysical Research Letters, 34(7), L07501, 2007.

Pouliquen, O., and Forterre, Y.: Friction law for dense granular flows: application to the motion of a mass down a rough inclined plane, Journal of fluid mechanics, 453, 133-151, 2002.

Preuth, T., Bartelt, P., Korup, O., and McArdell, B. W.: A random kinetic energy model for rock avalanches: Eight case studies. Journal of Geophysical Research: Earth Surface, 115, F03036, 2010.

Scaringi, G., Fan, X. M., Xu, Q., Liu, C., Ouyang, C. J., Domènech, G., Yang, F., and Dai, L. X.: Some considerations on the use of numerical methods to simulate past landslides and possible new failures: the case of the recent Xinmo landslide (Sichuan, China), Landslides, 15, 1359-1375, 2018

Schraml, K., Thomschitz, B., McArdell, B. W., Graf, C., and Kaitna, R.: Modeling debris-flow runout patterns on two alpine fans with different dynamic simulation models, Natural Hazards and Earth System Science, 15(7), 1483-1492, 2015.

Shugar, D. H., et al.: A massive rock and ice avalanche caused the 2021 disaster at Chamoli, Indian Himalaya. Science, 373, 300-306, 2021.

Sovilla, B., and Bartelt, P.: Observations and modelling of snow avalanche entrainment. Natural Hazards and Earth System Sciences, 2(3/4), 169-179, 2002.

Sovilla, B., McElwaine, J. N., & Köhler, A. (2018). The intermittency regions of powder snow avalanches. *Journal of Geophysical Research: Earth Surface*, *123*(10), 2525-2545.

Valero, C. V., Jones, K. W., Bühler, Y., & Bartelt, P.: Release temperature, snow-cover entrainment and the thermal flow regime of snow avalanches, Journal of Glaciology, 61(225), 173-184, 2015.

Voellmy, A.: Uber die zerstorungskraft von lawinen, Bauzeitung, 73, 159-165, 1955.

Walter, F., Amann, F., Kos, A., Kos, A., Kenner, R., Phillips, M., Preux, A., Huss, M., Tognacca, C., Clinton, J., Diehl, T., and Bonanomi, Y.: Direct observations of a three million cubic meter rock-slope collapse with almost immediate initiation of ensuing debris flows, Geomorphology, 351, 106933, 2020.

Wang, Y. F., Dong, J. J., and Cheng, Q. G.: Normal Stress-Dependent Frictional Weakening of Large Rock Avalanche Basal Facies: Implications for the Rock Avalanche Volume Effect, Journal of Geophysical Research: Solid Earth, 123, 3270-3282, 2018.

Zhao, S. X., He, S. M., Li, X. P., Scaringi, G., Liu, Y., and Deng, Y.: Investigating the dynamic process of a rock avalanche through an MLS-MPM simulation incorporated with a nonlocal μ(I) rheology model, Landslides, 2024. Doi: 10.1007/s10346-024-02244-6

Zhao, T., Crosta, G. B., Utili, S., and De Blasio, F. V.: Investigation of rock fragmentation during rockfalls and rock avalanches via 3-D discrete element analyses, Journal of Geophysical Research: Earth Surface, 122(3), 678-695, 2017.

Zhao, T., and Crosta, G. B.: On the dynamic fragmentation and lubrication of coseismic landslides. Journal of Geophysical Research: Solid Earth, 123,9914-9932, 2018.

Zhuang, Y., Yin, Y., Xing, A., and Jin, K.: Combined numerical investigation of the Yigong rock slide-debris avalanche and subsequent dam-break flood propagation in Tibet, China, Landslides, 17, 2217-2229, 2020.

Zhuang, Y, Xu, Q., Xing, A. G., Bilal, M., and Gnyawali, K. R.: Catastrophic air blasts triggered by large ice/rock avalanches, Landslides, 20, 53-64, 2023a.

Zhuang, Y., Xing, A., Sun, Q., Jiang, Y., Zhang, Y., and Wang, C.: Failure and disaster-causing mechanism of a typhoon-induced large landslide in Yongjia, Zhejiang, China, Landslides, 20(10), 2257-2269, 2023b.

Zhuang, Y., Piazza, N., Xing, A. G., Christen, M., Bebi, P., Bottero, A., Stoffel, L., Glaus, J., and Bartelt, P.: Tree Blow-Down by Snow Avalanche Air-Blasts: Dynamic Magnification Effects and Turbulence. Geophysical Research Letters, 50, e2023GL105334, 2023b.

Zhuang, Y., Dawadi, B., Steiner, J., Dash, R. K., Bühler, Y., Munch, J., and Bartelt, P.: An earthquake-triggered avalanche in Nepal in 2015 was exacerbated by climate variability and snowfall anomalies. Communications Earth & Environment, 5, 465, 2024.